Low-frequency spontaneous radiation in a free-electron laser in the trapped regime

W. Becker, J. K. McIver, and M. Orszag*
Center for Advanced Studies and Department of Physics and Astronomy, University of New Mexico, 800 Yale Boulevard N.E., Albuquerque, New Mexico 87131

P. Vogl†
Center for Nonlinear Studies, Los Alamos National Laboratory, Los Alamos, New Mexico 87545
(Received 3 August 1987)

The trapped regime of a free-electron laser is considered in terms of the relativistic quantum-mechanical Klein-Gordon equation in the presence of the undulator and the laser field. The electron which is trapped in the wells of the ponderomotive potential occupies discrete equidistant levels. Transitions between these quantum-mechanical levels are shown to lead to the well-known classical sidebands. As a new feature in spontaneous emission we obtain a low frequency $\delta\omega$ emitted slightly off axis, where $\delta\omega$ denotes the shift between the first sideband and the small-signal laser frequency. The low frequency is again classical and constitutes a sideband of the zeroth harmonic $\omega=0$. Under current experimental conditions this low-frequency spontaneous emission is at the borderline of detectability.

I. INTRODUCTION

The appearance of sidebands to the central signal frequency is considered a major obstacle for high-power operation of a free-electron laser (FEL). The sidebands are generated by electrons oscillating in the wells of the ponderomotive potential in which they are trapped at high laser intensity. They were first predicted a number of years ago,[1] then elaborated on and corroborated in numerical simulations,[2–6] and have recently been observed in the Compton regime[7] as well as in the Raman regime.[8] A great deal of progress has been made towards an analytical understanding of their properties.[9]

All previous work on the sidebands followed one of several classical approaches. In this paper we will take up again the quantum-mechanical point of view that was adopted in Madey's first derivation of the gain.[10] This is not because there is much that is quantum mechanical about them, although this may come as a surprise: after all, our starting point will be the quantized motion of an electron trapped in one of the wells of the periodic ponderomotive potential. The periodic potential gives rise to allowed and forbidden energy bands as in a solid. Near the bottom of the wells the overlap of wave functions localized at adjacent wells is so small that the allowed bands can for most practical purposes just be considered as discrete levels. Moreover, the potential not too far from its bottom is close to a harmonic oscillator, so that the levels are equidistant to an excellent approximation. One might then expect that electron transitions between these quantum levels should give rise to quantum-mechanical phenomena at least as long as one does not average over some initial level distribution. It will be amusing to see that this expectation is wrong. Rather, the transitions will generate the well-known and completely classical sideband instability even if it is assumed that the electron is initially in some definite level. We should mention that the assumption underlying the description in terms of energy bands, viz., an infinite extent of the periodic ponderomotive potential, is very well justified in practice since its period in space as well as time is essentially the period of the *optical* field. In comparison to this the length of the undulator is virtually infinite.

We shall start by briefly reviewing Madey's first derivation of the gain:[10] Let us first consider the electron traveling through the undulator in the absence of any laser field. The electron emits spontaneous radiation or, equivalently, classical bremsstrahlung, predominantly into a very narrow forward cone. These photons, once there, stimulate both emission of additional photons into the same mode and absorption of photons from this mode. The rates for emission and absorption are almost equal except that an electron with specified energy emits at slightly lower frequencies than it absorbs, because of the quantum-mechanical recoil. Gain is then proportional to the difference between the rates for emission and absorption. This difference is proportional to Planck's constant $\hbar$ (since the recoil is) thus canceling the $\hbar^{-1}$ inherent in the rate of spontaneous emission, so that the resulting gain is classical. This picture provides all the basic results of the small-signal regime, see e.g., Ref. 11. In this paper, we shall extend it beyond the small-signal regime.

As the laser field grows, the physical picture just outlined, viz., spontaneous emission due to the undulator field is stimulated by the photons already emitted, is no longer justified. Rather, as a next step, one now has to consider spontaneous emission due to the combined undulator *and* laser field. While the spontaneous spectrum in the small-signal regime consists (for circular polarization and on axis) just of the laser frequency, it now contains besides this original laser frequency additional upper and lower sidebands which are equally spaced in this case, where the electron is deeply trapped in the

wells of the ponderomotive potential. These are exactly the sidebands well known from the various classical approaches.[1-6] They originate from oscillations of the trapped electron inside its confining potential well. In the quantum-mechanical description, they stem from the electron making transitions between the equidistant levels of the harmonic oscillator by which the lower part of the ponderomotive potential is well approximated. Gain can be computed as before: As soon as the sideband modes are populated with photons further emission into and absorption from these modes is stimulated, and gain can be inferred from the difference. Again, as those sidebands which have positive gain grow and reach a certain intensity, they will modify spontaneous emission and generate sidebands to the sidebands, etc., until finally a spectrum without any discernable regular pattern evolves. This has been observed in computer simulations of the classical theory.[4]

Not surprisingly, the higher stages of this hierarchy of sideband generation become intractable with analytical methods. In this paper we shall concentrate on the first stage beyond the small-signal regime, i.e., the generation of sidebands due to the original laser field after it has grown strong enough to trap the electrons. In particular, we shall concentrate on what we call "sidebands to the zeroth harmonic," a feature of the spectrum which, although entirely classical, seems to have escaped attention in the classical description. By this we mean the following: the sidebands known from previous work are sidebands to the left and right of the original (i.e., essentially the small-signal) laser frequency. However, it turns out that the zeroth harmonic $\omega=0$ develops sidebands, too. These latter ones originate from purely longitudinal oscillations of the electron in the ponderomotive potential. Hence, they are only emitted off axis, although, due to the highly relativistic speed of the electron, very close to the forward direction. Formally, they owe their existence to the $\mathbf{p}\cdot\mathbf{A}$ term in the interaction Lagrangian (which does not contribute on the axis). In contrast, the ordinary sidebands come from longitudinal oscillations superimposed on transverse ones and, formally, from the $\mathbf{A}^2$ term.

The formal framework for the program outlined above is provided by the solutions of the Klein-Gordon equation in the presence of the undulator *and* the laser field, both being treated as prescribed classical fields. Neglecting the electron's spin is an excellent approximation, as spin-dependent corrections are typically of the order of $(\hbar\omega/mc^2\gamma)^2$ which is of the order of 10^{-16} for typical FEL's.[12] We shall here only consider circular polarization. In the mere presence of the undulator field the solutions of the Klein-Gordon equation are on axis just exponentials. With the additional presence of the laser field the solutions are Mathieu functions. Analytic approximations for these functions are available for all regimes of their parameters.[13] These would, in principle, allow one to follow the evolution of the sidebands from very low intensities of the laser field (where they are absent) up to the deeply trapped regime. However, except for these two limiting cases, the approximations are unwieldy and one might be better served with numerical methods. In this paper, we will be content with the limiting case of the deeply trapped regime where the Mathieu functions can be approximated by Hermite polynomials (i.e., harmonic-oscillator functions).

In Sec. II we discuss the Klein-Gordon equation of the present problem and its solution in terms of Mathieu functions. We also present the analytical approximations which we will use in order to deal with them. In Sec. III we consider the general matrix element which describes spontaneous emission due to the combined undulator and laser field. We extract the well-known sideband spectrum and, in addition, the above-mentioned sidebands to the zeroth harmonic. In Sec. IV we evaluate spontaneous emission of this zeroth-order sideband. Calculational details are given in the Appendix. We do not, actually, calculate the gain of the various sidebands, but are content with discussing qualitatively, in Sec. V, some points in which the calculation differs from the corresponding one in the small-signal regime. Finally, we summarize our conclusions.

II. WAVE FUNCTIONS IN THE PRESENCE OF THE UNDULATOR AND THE LASER FIELD

In the semiclassical approach to be used we start from the Klein-Gordon equation

$$\left[\frac{1}{c^2}\left[i\hbar\frac{\partial}{\partial t}-eA_0\right]^2-\left[i\hbar\nabla+\frac{e}{c}\mathbf{A}\right]^2-m_e^2c^2\right]\phi=0\ . \tag{1}$$

The external field is the sum of the static undulator field

$$\mathbf{A}_W=a_W[\hat{\mathbf{x}}\cos(\omega_0 z/c)+\hat{\mathbf{y}}\sin(\omega_0 z/c)]\ , \tag{2}$$

with period $\lambda_0=2\pi c/\omega_0$ and the laser field

$$\mathbf{A}_L=a_L[\hat{\mathbf{x}}\cos\omega(t-z/c)+\hat{\mathbf{y}}\sin\omega(t-z/c)]\ , \tag{3}$$

with wavelength $\lambda=2\pi c/\omega$ propagating in the positive z direction, and we consider, for simplicity, the case of circular polarization. In Eq. (1), then, $\mathbf{A}=\mathbf{A}_L+\mathbf{A}_W$ and $A_0=0$. It is convenient to introduce the dimensionless variables[14]

$$u=\omega t-(\omega+\omega_0)z/c,\quad v=(\omega+\omega_0)t-\omega z/c\ , \tag{4}$$

and the conjugate momenta

$$p_u=\frac{\omega E-(\omega+\omega_0)pc}{\hbar\omega_0(\omega_0+2\omega)},\quad p_v=\frac{(\omega+\omega_0)E-\omega pc}{\hbar\omega_0(\omega_0+2\omega)}\ , \tag{5}$$

replacing the electron's total energy E and its axial canonical momentum p. The variable v plays the role of time, because the planes $v=$const are spacelike. The introduction of the variables (4) and (5) is essentially equivalent to the transition to the comoving Bambini-Renieri frame,[15] where the resonant electron is at rest. This becomes clear if one notices that $p_u=0$ corresponds to

$$\beta=\frac{pc}{E}=\frac{\omega}{\omega+\omega_0}\ ,$$

which is the velocity of the resonant electron. Equivalently, one can see that $du/dt=0$ if

$$\frac{dz}{dt}=c\frac{\omega}{\omega+\omega_0} .$$

The variables v and p_v are then chosen so that $(tE-zp)/\hbar=vp_v-up_u$. The axial canonical momentum p is understood in the presence of the undulator field so that

$$cp=[E^2-m_e^2c^4-(ea_W)^2]^{1/2} . \tag{6}$$

In terms of the variables (4) the Klein-Gordon equation (1) assumes the form

$$\left[\frac{1}{c^2}\omega_0(\omega_0+2\omega)\left[\frac{\partial^2}{\partial u^2}-\frac{\partial^2}{\partial v^2}\right]+\nabla_T^2-\frac{2ie}{\hbar c}\mathbf{A}\cdot\nabla_T -\frac{e^2}{\hbar^2c^2}(a_L^2+a_W^2+2a_La_W\cos u)-\left[\frac{m_e^2}{\hbar}\right]^2\right]\phi=0 . \tag{7}$$

Here the gradient ∇_T is with respect to the two transverse variables $\mathbf{x}_T=(x,y)$, and the corresponding transverse canonical momentum will be denoted by $\mathbf{p}_T=(p_x,p_y)$. We will be interested in the case where the electron initially propagates on axis, $\mathbf{p}_T=0$, then emits a photon in an arbitrary direction so that the final electron momentum $\mathbf{p}'_T$ is not necessarily on axis. However, because of momentum conservation $\mathbf{p}'_T+\hbar\mathbf{k}_T=\mathbf{p}_T=0$ with $\mathbf{k}$ the wave vector of the emitted photon. Hence $|\nabla_T|\sim\hbar^{-1}|\mathbf{p}'_T|=|\mathbf{k}'_T|$, and we may neglect the gradient terms even for the final electron, since we consider intense fields ($ea_W/m_ec^2\sim1$, $ea_L/m_ec^2\sim10^{-2}$) so that the gradient terms are comparatively small. Under these conditions the interaction term in Eq. (7) depends only on the variable u (the term $\mathbf{A}\cdot\nabla_T$ would depend on v, too) so that the momentum p_v is conserved.

The solution of Eq. (7) is now

$$\phi=(2p_vL_T^2L_u)^{-1/2}e^{(-ivp_v+i\mathbf{p}_T\cdot\mathbf{x}_T)/\hbar}me_\nu(u/2,h^2) , \tag{8}$$

where me_ν is a solution of Mathieu's equation

$$\left[\frac{\partial^2}{\partial\xi^2}+\lambda-2h^2\cos(2\xi)\right]me_\nu(\xi,h^2)=0 . \tag{9}$$

We will follow the conventions of Ref. 14. The parameters λ and h^2 are given by

$$\lambda=4\left[p_v^2-\frac{m_*^2c^4}{\hbar^2\omega_0(\omega_0+2\omega)}\right] , \tag{10}$$

$$m_*^2c^4=m_e^2c^4+e^2(a_W^2+a_L^2) , \tag{11}$$

$$h^2=\frac{4e^2a_Wa_L}{\hbar^2\omega_0(\omega_0+2\omega)} . \tag{12}$$

We notice for later use that λ may also be expressed in terms of the momentum component p_u which is proportional to the detuning from resonance:

$$\lambda=4\left[p_u^2-\frac{e^2a_L^2}{\hbar^2\omega_0(\omega_0+2\omega)}\right] , \tag{13}$$

$$p_u=\frac{m_e\gamma\,\Delta\omega\,c^2}{\hbar\omega_0(\omega_0+2\omega)} , \tag{14}$$

$$\Delta\omega=\omega-(\omega+\omega_0)\beta_0 , \tag{15}$$

where $\beta_0=cp/E$ is the longitudinal velocity of the electron in the undulator.

The Mathieu functions here take the place of the Jacobian elliptic functions which appear in the classical formulation of the problem.[9] Analytical approximations for the Mathieu functions are available throughout the entire range of the parameters λ and h^2.[13] In general, these may be quite complicated. However, here we will be satisfied with considering deeply trapped electrons. In this case, which corresponds to the limit $h\to\infty$, the Mathieu functions essentially become harmonic-oscillator functions. The explicit expressions will be given below. We first notice that the Mathieu functions have the Floquet-Bloch expansion

$$me_\nu(\xi,h^2)=e^{i\nu\xi}\sum_{r=-\infty}^{\infty}c_{2r}^\nu(h^2)e^{2ir\xi} . \tag{16}$$

Here the characteristic index $\nu=\nu(\lambda,h^2)$ is a function of λ and h^2 and may be real or complex. The exponentially growing behavior of the solutions with complex ν is unacceptable, and they have to be discarded. In the deeply trapped regime, where $h\to\infty$, this leaves us with practically discrete levels, viz., the harmonic-oscillator levels which originate from the parabolic approximation to the ponderomotive potential [the $\cos u$ term in Eq. (7)]. For real ν and $h\to\infty$, the connection between λ,h^2 and ν is given by[16,17]

$$\lambda=\lambda_\nu(h^2) =-2h^2+2(2m+1)h-\tfrac{1}{8}[(2m+1)^2+1] -\frac{1}{128h}[(2m+1)^3+3(2m+1)]+O(m^4/h^2) , \tag{17}$$

with $m=[|\nu|]$ the largest integer smaller than $|\nu|$. The equidistant harmonic-oscillator levels arise for $m\gg1$ in a linear expansion of Eq. (17) about a particular value of m [corresponding via Eqs. (10) and (5) to a particular electron energy or momentum]. The entire situation is illustrated in Fig. 1 which depicts the so-called stability chart. An example of the corresponding levels in the ponderomotive potential is given in Fig. 2. An estimate of the value of m that corresponds to a trapped electron is obtained as follows: The quantity ea_L/m_ec^2 is rather small, for example, for the Los Alamos experiments[7] it is of the order of 10^{-3}. In view of this, Eq. (13) implies that $\lambda>0$ if $\Delta\omega T\sim1$ (T being the undulator transit time). In any event, we will have that $|\lambda|\ll2h^2$. Equation (17) then says that $m>h/2$ in order to compensate the large negative term of $-2h^2$ on the right-hand side. On the other hand, we will always have that $|p_u|\ll p_v$. Hence $m\sim h/2$ is a sufficiently accurate estimate to be used later on.

Again, for $h \to \infty$, the expansion coefficients in Eq. (16) may be approximated by[16,17]

$$c_{2r}^{\nu}(h^2) \cong (-1)^r \left[\frac{2}{\pi h}\right]^{1/4} (2^m m!)^{-1/2} e^{-(2r+\nu)^2/4h} \times H_m\left[\frac{2r+\nu}{\sqrt{2h}}\right], \tag{18}$$

where again $m = [\,|\nu|\,]$ and the H_m are Hermite polynomials. Equations (16), (17), and (18) allow us to deal with the Mathieu functions in the regime of interest. We finally notice that the square root in Eq. (8) serves to normalize the wave function $\phi(u,v,\mathbf{x}_T)$ to unity for constant "time" v,

$$i \int_{-L_T/2}^{L_T/2} d^2\mathbf{x}_T \int_{-L_u/2}^{L_u/2} du\, \phi(u,v,\mathbf{x}_T)^* \times \left[\frac{\vec{\partial}}{\partial v} - \frac{\overleftarrow{\partial}}{\partial v}\right] \phi(u,v,\mathbf{x}_T) = 1 . \tag{19}$$

In order to verify this, the relation

$$\sum_{r=-\infty}^{\infty} [c_{2r}^{\nu}(h^2)]^2 = 1$$

is needed.

III. GENERAL DISCUSSION OF THE MATRIX ELEMENT

We now proceed to evaluate the matrix element

$$M = e\left[\frac{2\pi c^2}{\hbar\Omega V}\right]^{1/2} \int dz \int dt\, d^2x_T \left[\phi_f^*(u,v,\mathbf{x}_T)\left[i\boldsymbol{\epsilon}\cdot(\vec{\nabla}-\overleftarrow{\nabla}) - \frac{2e}{\hbar c}(\mathbf{A}_L + \mathbf{A}_W)\cdot\boldsymbol{\epsilon}\right]\phi_i(u,v,\mathbf{x}_T)\right] e^{i(\Omega t - \mathbf{K}\cdot\mathbf{x})} , \tag{20}$$

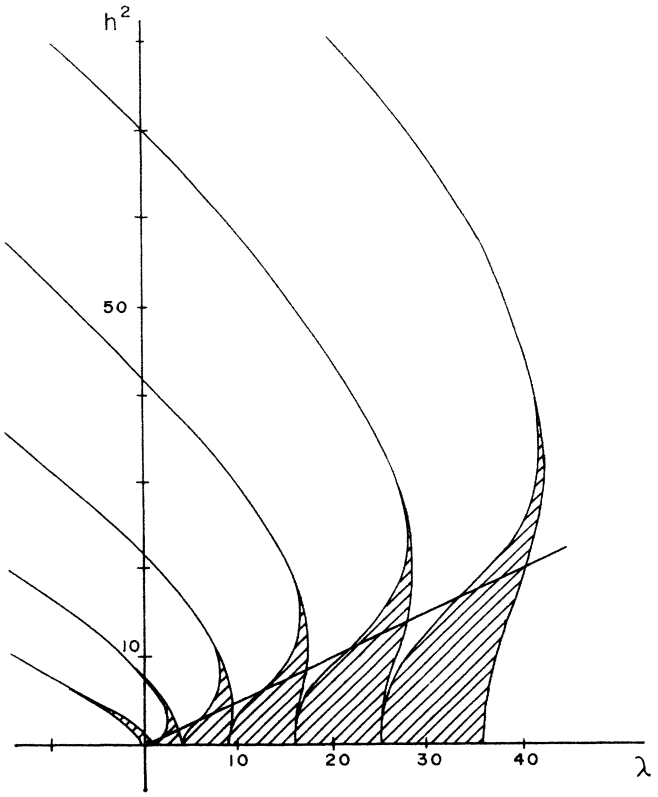

FIG. 1. The stability chart of the Mathieu functions. The (λ,h^2) plane is divided into stable and unstable regions according to whether $\nu = \nu(\lambda,h^2)$ is real or not. The stable areas are hatched. For $h^2 \ll \lambda$, stable behavior predominates, for $h^2 \gg \lambda$ the stable regions have shrunk into virtually discrete levels in agreement with Eq. (17). The straight line $\lambda = 2h^2$ is the division line between the predominantly stable and unstable part of the (λ,h^2) plane. It corresponds to the maxima of the ponderomotive potential (cf. Fig. 2).

which describes the spontaneous emission of a quantized photon with frequency Ω, wave vector $\mathbf{K}$, and polarization $\boldsymbol{\epsilon}$ by an electron with the wave function ϕ_i (specified by the momenta $p_v, \mathbf{p}_T = 0$, and the characteristic index ν) so that the electron in the final state has the wave function ϕ_f (specified by p_v', $\mathbf{p}_T'$, and ν'). The two terms on the right-hand side (rhs) of Eq. (20) originate from the $\mathbf{p}\cdot\mathbf{A}$ term and the $\mathbf{A}^2$ term in the interaction Hamiltonian of scalar quantum electrodynamics (see, e.g., Ref. 18; for the application of scalar QED to the FEL, see Ref. 19). Before getting into the detailed evaluation of the matrix element let us first evaluate the emitted frequencies Ω for emission on axis in the positive z direction. The line centers are obtained by integrating over all space and time. This yields two δ functions for the u and v components implying

$$p_v' - p_v + [\Omega - (\alpha+\beta)\omega]/(\omega_0 + 2\omega) = 0 , \tag{21}$$

$$\tfrac{1}{2}(\nu - \nu') + \rho + [\Omega - (\alpha+\beta)\omega - \beta\omega_0]/(\omega_0 + 2\omega) = 0 . \tag{22}$$

Here ρ is any integer, and for a photon emitted via the coupling term $\boldsymbol{\epsilon}\cdot\nabla$ in Eq. (20) one has to take $\alpha = \beta = 0$; for emission via the term $\boldsymbol{\epsilon}\cdot\mathbf{A}_L$, $\beta = 0$ and $\alpha = 1$ or $\alpha = -1$; for emission via the $\boldsymbol{\epsilon}\cdot\mathbf{A}_W$ term $\alpha = 0$ and $\beta = +1$ or $\beta = -1$.

The initial state of the electron is specified by given values of p_v and ν. This implies that the electron is in the mth band (or rather level) with $m = [\,|\nu|\,]$. From Eq. (21) the emitted frequency is

$$\Omega = (\alpha+\beta)\omega - (\omega_0 + 2\omega)(p_v' - p_v) . \tag{23}$$

The possible values of p_v' are related to the index m' characterizing the final level of the electron. Since $p_v \gg 1$ and $m \gg 1$, we have to an excellent approximation

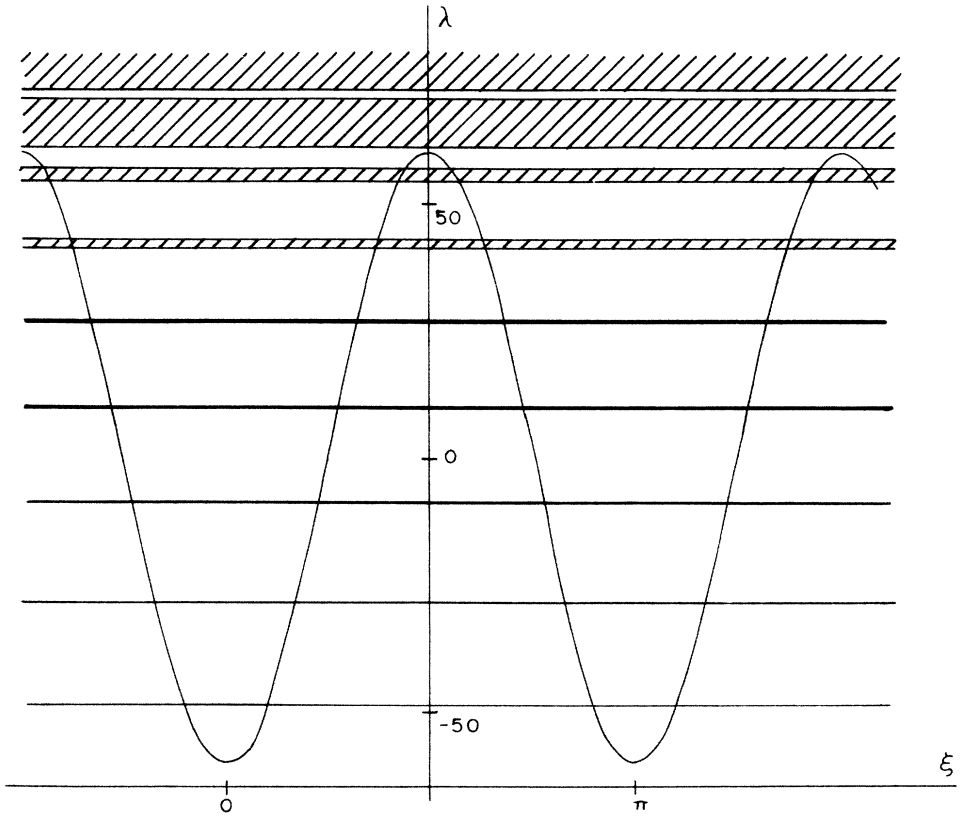

FIG. 2. The stable bands in the ponderomotive potential $-2h^2\cos(2\xi)$ are represented by the hatched areas. The figure illustrates the transition from virtually discrete levels near the bottom of the potential to an (almost) continuum for $\lambda \gg 2h^2$. The figure is for $h^2=30$. For the large values of h^2, which are of interest in this paper, the sequence of stable and unstable bands is much closer.

$$p_v'-p_v \cong \frac{1}{2p_v}(p_v'^2-p_v^2)=\frac{1}{8p_v}(\lambda'-\lambda)$$
$$\cong \frac{1}{8p_v}(4h-m)(m'-m)\ , \qquad (24)$$

where Eqs. (10) and (17) have been used and we only kept the first three terms on the rhs of Eq. (17). The emitted frequency then is

$$\Omega=(\alpha+\beta)\omega-\frac{(\omega_0+2\omega)(4h-m)}{8p_v}(m'-m)\ . \qquad (25)$$

Here the quantity $m'-m$ can have, in principle, arbitrary positive or negative integer values. We shall see below, however, that only the even integer values $m'-m=2\rho$ actually play a role. In any event, for $\alpha+\beta=1$, which is the case for emission due to the $\mathbf{A}^2$ term (the case $\alpha+\beta=-1$ leads to a negative frequency in emission and, consequently, does not contribute to emission; it does contribute to absorption), Eq. (25) specifies a sequence of equally spaced sidebands on either side of the original laser frequency ω. Although in the present picture the sidebands are generated by electron transitions between the discrete levels of a quantized harmonic oscillator, they are identical with the well-known sidebands obtained from the classical analysis. In fact, the expression (25) is independent of $\hbar$, since

$$h/p_v=2[e^2a_W a_L/(m_*^2c^4)]^{1/2} \qquad (26)$$

is independent.

For emission due to the $\mathbf{p}\cdot\mathbf{A}$ term we have $\alpha+\beta=0$, and there are sidebands to the "zeroth harmonic" $\omega=0$. Although these are of classical origin as well, they have apparently not been noticed in the classical analysis. Typically, $h/p_v=10^{-2}-10^{-1}$, hence this constitutes emission into a frequency range very different from the laser frequency ω. We notice, that the $\mathbf{p}\cdot\mathbf{A}$ term does not produce emission on axis since $\mathbf{p}'\cdot\boldsymbol{\epsilon}=-\hbar\mathbf{K}\cdot\boldsymbol{\epsilon}=0$ for $\mathbf{K}=K\hat{\mathbf{z}}$. Hence, this low frequency radiation is only emitted off axis. In the rest of this paper, we will be mainly concerned with these "zeroth-order" sidebands. First, however, we still have to discuss the possible values of the integer m' which determines the level of the final electron.

Equation (22) fixes the value of ν' for the final electron. With the frequency Ω substituted from Eq. (25) it now reads

$$\tfrac{1}{2}(\nu-\nu')+\rho-\frac{4h-m}{8p_v}(m'-m)-\frac{\beta\omega_0}{\omega_0+2\omega}=0\ . \qquad (27)$$

In general, we will have $\omega \gg \omega_0$, $p_v \gg 1$, and $m \approx h/2$, so that the last two terms in Eq. (27) are small corrections. Let us first consider the case where $m'=m$, i.e., no sidebands are emitted and the electron remains in its original level. Recalling that $m=[\,|\nu|\,]$ we infer that $0<\nu-\nu'<1$. Equation (27) then has the consequence that $\rho=0$ and $\nu'=\nu+O(\omega_0/\omega)$ for $\beta=1$, or $\nu'=\nu$ for $\beta=0$. Next consider $m'=m-1$ corresponding to the lowest possible upper sideband and the electron dropping by one level. In this case $0<\nu-\nu'<2$. One can readily convince oneself that Eq. (27) now requires that $\rho=-1$ and $\nu-\nu'=2-O(h/p_v)$. As long as $h/p_v \ll 1$ this can only be satisfied if the initial state of the electron is such that the value of ν is very close to $m+1$. If the electrons are equally distributed over all available states, only very few electrons will satisfy this condition. We therefore conclude that the sideband corresponding to $m'=m-1$, although present in principle, will be strongly suppressed. Notice, however, that for increasing values of h/p_v this suppression becomes less effective. The same reasoning applies for the lowest possible lower sideband ($m'=m+1$) and, in fact, whenever m' and m differ by an odd integer. In contrast, for $m'=m-2$ we have $1<\nu-\nu'<3$ and Eq. (27) yields $\rho=-1$ and $\nu-\nu'=2-O(p_v^{-1})$. This latter condition is readily satisfied for almost all electron levels. Again, the same argument applies whenever m' and m differ by an even integer. The preceding discussion is illustrated in Fig. 3. It can be summarized by stating that sidebands will be observed corresponding to $m'-m=2\rho$ with the frequencies

$$\Omega \cong (\alpha+\beta)\omega - 2\rho\frac{h}{p_v}\omega \quad (\rho=0,\pm1,\pm2,\cdots)\,, \tag{28}$$

where $\alpha+\beta$ equals zero or unity. This is the standard result for the sideband frequencies[1–6] except that the possibility that $\alpha=\beta=0$ apparently went unnoticed.

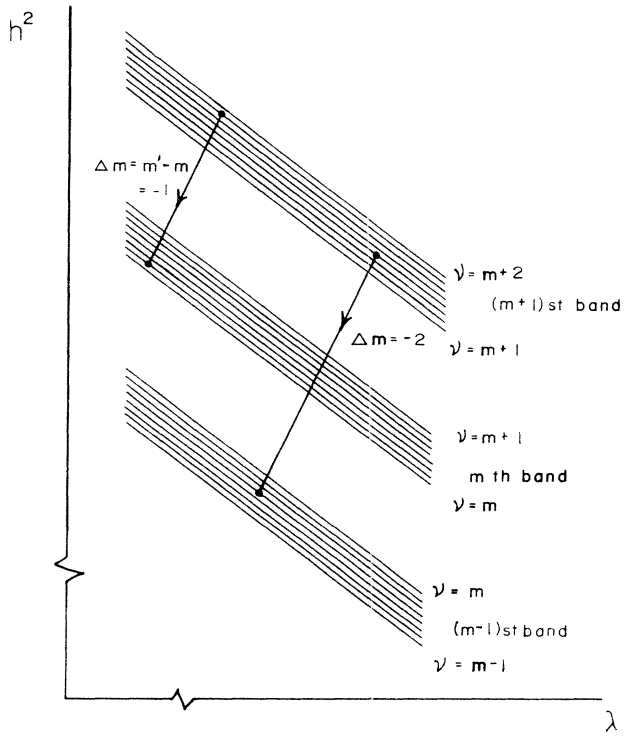

FIG. 3. This is, in principle, an enlargement of a region of Fig. 1 where $h^2 \gg \lambda$ so that the stable bands are practically discrete levels. The figure is not to scale, i.e., the extent of the bands is strongly exaggerated so as to show that the bands actually consist of levels characterized by a given value of ν. In the mth band, ν varies from a lower value of m up to $m+1$. [We here ignore mathematical subtleties such as whether me_m corresponds to $\nu=m$ in the $(m-1)$th band or $\nu=m$ in the mth band. For these questions which are irrelevant for the present paper we refer to the literature.] In view of Eq. (27), transitions such that $m'=m-1$ (implying $0<\nu-\nu'<2$) are only possible if the initial state of the electron is very near the top of a band. No such restrictions apply for transitions such that $m'=m-2$.

IV. EMISSION OF ZEROTH-ORDER SIDEBANDS

We now turn to the evaluation of the matrix element (17) for emission of the zeroth-order sidebands. As mentioned before, these are only emitted off axis. They originate from the term proportional to $\epsilon\cdot(\vec{\nabla}-\overleftarrow{\nabla})$, so from now on we shall concentrate on this term. The evaluation is rather straightforward. Hence we just give the result and relegate some calculational details to the Appendix. We are only interested in the total rate of emission into a given sideband, not in the line shape [this would have the usual $(\sin x/x)^2$ form]. Hence we may integrate in Eq. (20) over all space and time. We also sum over the final states of the electron and the energy and polarization of the emitted photon within the considered sideband. The differential rate of emission of the sideband numbered by ρ into the solid angle element $d\Omega_{\mathbf{K}}$ per unit "time" L_v then is

$$dR_\rho = \frac{d\Omega_{\mathbf{K}}}{L_v}\int\int\frac{d^2p_T\,dp_v'}{(2\pi)^3}L_T^2L_u\frac{V\Omega^2 d\Omega}{(2\pi)^3}\,|M_\rho|^2$$
$$=\frac{2e^2}{\pi\hbar c}\frac{\Omega^4\sin^2\vartheta}{|\rho|\,[\omega_0(\omega_0+2\omega)]^2(\nu'-\nu-2\rho)^2}$$
$$\times[J_{2\rho}((m/h)^{1/2}(\nu'-\nu-2\rho))]^2 d\Omega_{\mathbf{K}}\,, \tag{29}$$

and the now angular dependent frequency is

$$\Omega \cong -2\rho\frac{h}{p_v}\frac{\omega_0}{\omega_0+\frac{1}{2}\vartheta^2\omega}\omega\,. \tag{30}$$

The exact expression is given in Eq. (A7). For small angles $\vartheta \ll 1$, the argument of the Bessel functions is [cf. Eqs. (A6) and (A8)]

$$\left(\frac{m}{h}\right)^{1/2}(\nu'-\nu-2\rho) = -2\rho\frac{\sqrt{mh}}{p_v}\frac{\omega_0-\frac{1}{2}\vartheta^2\omega}{\omega_0+\frac{1}{2}\vartheta^2\omega}\,. \tag{31}$$

Since $m \sim h/2$ and $h \ll p_v$, the Bessel function may be approximated by the leading term of its power-series expansion so that

$$dR_\rho = \frac{e^2}{8\pi\hbar c}\left[\frac{m}{h}\right]^{2\rho}\rho^{4\rho-1}\left[\frac{h}{p_v}\right]^{4\rho+2} \times(2\omega\omega_0)^2\sin^2\vartheta\frac{(\omega_0-\frac{1}{2}\vartheta^2\omega)^{4\rho-2}}{(\omega_0+\frac{1}{2}\vartheta^2\omega)^{4\rho+2}}d\Omega_{\mathbf{K}} , \quad (32)$$

where ρ stands for $|\rho|$. In view of the factor of $(h/p_v)^{4\rho+2}$ the emission of zeroth-order sidebands with $\rho > 1$ quickly becomes insignificant. There is no emission of any sidebands at $\vartheta = 0$ and $\vartheta_0 = (2\omega_0/\omega)^{1/2}$. For angles $\vartheta > \vartheta_0$ the emitted frequency decreases rapidly. Therefore, a reasonable quantity to calculate is the number of photons per electron and time L_v emitted into the cone $\vartheta < \vartheta_0$. This is, for $\rho = -1$,

$$\int_{\vartheta=0}^{\vartheta=\vartheta_0} dR_{-1} = \frac{\pi e^2}{2\hbar c}\left[\frac{m}{h}\right]^2\left[\frac{h}{p_v}\right]^6\left[\frac{2\omega}{\omega_0}\right]^{1/2}\left[\ln 2 - \frac{83}{120}\right] . \quad (33)$$

The transit time L_v for an electron to travel through the undulator follows from the definition (4) of the variable v,

$$L_v = (\omega+\omega_0)T - \omega\beta_0 T \cong 2\omega_0 T \cong 2\omega_0 n\lambda_0/c = 4\pi n , \quad (34)$$

where T is the passage time (real time) through the undulator, $\beta_0 \cong 1 - 1/2\gamma_0^2$ the axial velocity of the electron, and n the number of undulator periods. The number of photons of the lowest zeroth-order sidebands ($\rho = -1$) emitted into the cone $\vartheta < \vartheta_0$ by one electron traveling through the undulator finally is

$$N_1 = 4\pi^2 n\gamma_0\frac{e^2}{\hbar c}\left[\frac{m}{h}\right]^2\left[\frac{h}{p_v}\right]^6(1.5\times10^{-3}) . \quad (35)$$

The quantity h/p_v decides about the order of magnitude of this expression. It can be estimated from Eq. (26) in terms of the undulator parameter $ea_W/m_e c^2$ and the corresponding quantity $ea_L/m_e c^2$ for the laser field. Alternatively, with the help of Eq. (28) it may be expressed in terms of the frequency difference between the ordinary laser frequency and the first sideband for $\vartheta = 0$,

$$\frac{h}{p_v} = \frac{1}{2}\frac{\delta\omega}{\omega}, \quad \delta\omega = \Omega(\rho=1, \vartheta=0) - \omega . \quad (36)$$

The number N_1 per electron is quite small. For example, parameters typical of the Los Alamos experiments[7] are $n = 37$, $\gamma_0 = 34$, and $\delta\omega/\omega \sim 0.03$ for a laser intensity of 65 MW. This leads to $N_1 = 1.5\times10^{-12}$. During one macropulse, which contains 2000 micropulses each 36 ps long with a peak current of 40 A,[20] some 2×10^{13} electrons pass through the undulator. Hence we can expect about a dozen of the low-energy photons to be emitted during each macropulse.

V. REMARKS ON THE GAIN OF THE SIDEBANDS

The computation of the gain of the sidebands is rather straightforward and follows the outline given in the Introduction. The gain of the zeroth-order sideband is of little interest since owing to its low frequency it will normally suffer comparatively high losses at the mirrors (which are chosen to yield high reflection for the operating mode) and since, moreover, it is not strictly emitted on axis. The gains of the normal sidebands have recently been evaluated[9] in terms of Jacobi elliptic functions which take the place of the Mathieu functions in a classical description. These results are largely analytical, and we would have little to add to them. We therefore skip the actual evaluation of the gain and will be content with just a few remarks.

If the gain is to be evaluated as the difference between the rates of emission and absorption, one is tempted in analogy with the procedure in the small-signal case first to identify the quantum recoil. As it turns out, no recoil becomes visible, i.e, an electron, which occupies a given level in the ponderomotive potential well, emits and absorbs exactly the same frequency, in contrast to the small-signal regime. At second thought, this is not surprising, since unlike the free electron the bound electron cannot freely change its momentum but is restricted to the virtually discrete levels of the periodic ponderomotive potential. It turns out, however, that the rates of emission and absorption which are now centered at the same frequency are not equal so that a nonzero gain results as in the small-signal regime. Several qualitative features of the gain then emerge in agreement with the classical theory of Ref. 9: (a) For the electron in a specified initial level, gain as a function of frequency is strictly antisymmetric about the original input laser frequency; (b) in particular, the gain at the input frequency vanishes; (c) gain is predominantly positive on the low-frequency side of the input frequency; (d) the one-electron gain for fixed electron energy (i.e., for a given level) can be written as a derivative with respect to the electron energy. The gain due to an electron beam with a certain energy distribution is then (after an integration by parts) proportional to the derivative of this distribution with respect to energy.

In previous work the gain in the strong-field regime was calculated starting from the same Klein-Gordon equation (1), in the presence of the undulator field (2) and the laser field (3).[14,21] The presence of sidebands had not been noticed then, although they were implicit in the approach. A nonzero gain had been obtained in these earlier papers. The question arises of how this is compatible with the result of this paper that the gain at the input frequency vanishes. The answer lies in the observation that in Refs. 14 and 21 the energy loss of the electron was actually calculated and gain was inferred via energy conservation assuming the presence of just the input laser mode. If this is taken into account, the two calculations are compatible, i.e., the energy loss of the electron is due to the sidebands rather than the central frequency.

VI. CONCLUSIONS

We have extended Madey's first quantum-mechanical treatment of the free-electron laser, which is based on the competition between stimulated emission and absorption as derived from spontaneous emission, into the high-intensity trapped regime. The procedure lends itself to an appealing physical picture: spontaneous emission is in the initial stages just caused by the undulator field. This yields the small-signal regime laser mode. The latter while growing starts to alter spontaneous emission. Sidebands develop. Those which have grown will in turn influence spontaneous emission leading to a more complicated pattern of sidebands. Again those with positive gain will grow, etc. Thus a hierarchy of sidebands develops which will ultimately result in a chaotic pattern. In this paper we have concentrated on the first step beyond the small-signal regime where spontaneous emission due to the combined undulator and (small-signal) laser field is considered. In this first step the well-known equally spaced sidebands to the left and right of the original (small-signal) laser frequency are obtained. Two additional features emerged. (1) For increasing intensity sidebands should start showing up at half the normal frequency. These can only be emitted by electrons which are initially very near the top of one of the bands in the periodic ponderomotive potential. Since only few electrons satisfy this condition, these sidebands should be suppressed but present. (2) The zeroth harmonic $\omega=0$ develops side bands as well, with the same spacing as the sidebands of the original laser frequency. These sidebands are due to the $\mathbf{p}\cdot\mathbf{A}$ term in the interaction Hamiltonian and, consequently, are emitted slightly off axis. For present FEL's, this emission is very weak but might be detectable. The emission rate for the first sideband of $\omega=0$ is proportional to $(\delta\omega/\omega)^6$, where ω is the normal laser frequency and $\delta\omega$ the normal sideband spacing. Hence it will rapidly increase with higher intensity, viz., higher values of $\delta\omega/\omega$. Since the zeroth-harmonic sideband is emitted off axis and in a frequency regime very different from the operating frequency it is very unlikely that it would be amplified. Hence it would under all circumstances be observed in spontaneous emission. In a situation where it is sufficiently intense, it might then be a valuable diagnostic tool, since it provides information about the sideband spectrum which is not distorted by gain.

The calculations in this paper were based on lowest-order quantum-mechanical perturbation theory. They started from the discrete level structure of the electron which is deeply trapped by the ponderomotive potential. This level structure is not destroyed by any finite size effects such as the finite length of the undulator. Nevertheless, transitions between these levels do not lead to any quantum-mechanical effects. The effects just mentioned are classical, as are the sidebands which are familiar from the classical theory. The same conclusions should also apply to the motion of electrons in standing-wave fields, i.e., the situation considered by Kapitza and Dirac.[22] In this case the electron also experiences discrete levels very similar to those considered here.[23] Again, the radiation emitted or absorbed as a consequence of transitions between these levels should be essentially classical. We emphasize once more that this conclusion holds even when the electron occupies a well-defined quantum level. Finally, we mention that the same pattern of sidebands can be expected in free-electron devices which exploit stimulated Cerenkov radiation, since it can be shown[24] that they can be described by the same Hamiltonian as the ordinary FEL.

ACKNOWLEDGMENT

This work was supported in part by the U.S. Office of Naval Research.

APPENDIX

In this appendix we will deal with some details of the evaluation of the matrix element (20). It is convenient to perform the integration in terms of the variables u and v rather than z and t. The explicit form (8) of the wave functions along with the Floquet-Bloch expansion (16) of the Mathieu functions then enable one to perform all integrals in terms of δ functions. One is then left with quadratic sums of the expansion coefficients $c^{\nu}_{2r}(h^2)$:

$$A_\rho=\sum_{r=-\infty}^{\infty} c^{\nu'}_{2(r-\rho)}(h^2)c^{\nu}_{2r}(h^2) \tag{A1}$$

and

$$B_\rho=\sum_{r=-\infty}^{\infty} 2rc^{\nu'}_{2(r-\rho)}(h^2)c^{\nu}_{2r}(h^2)\ , \tag{A2}$$

where the integer ρ occurs in the argument of the δ function and specifies the particular sideband. The sums over r can be carried out in the limit of large h^2, where the asymptotic form (18) can be used, by converting the sum into an integral. The result is

$$A_\rho=\alpha L_m^{m'-m}(x^2)\ , \tag{A3}$$

$$B_\rho=\alpha\left[\frac{2h(m+1)}{\nu'-\nu-2\rho}L_{m+1}^{m'-m-1}(x^2)+\tfrac{1}{2}(\nu'-\nu-2\rho)L_{m-1}^{m'-m+1}(x^2)-\nu L_m^{m'-m}(x^2)\right], \tag{A4}$$

where

$$\alpha=(-1)^\rho(2^{m-m'}m!/m'!)^{1/2}(\sqrt{2}x)^{m'-m}\exp(-x^2/2)\ , \tag{A5}$$

$$x=(\nu'-\nu-2\rho)/2\sqrt{h}=\Omega\frac{(\omega+\omega_0)\cos\vartheta-\omega}{\sqrt{h}\,\omega_0(\omega_0+2\omega)}\ , \tag{A6}$$

and $m=[\,|\nu|\,]$, $m'=[\,|\nu'|\,]$, and the L_m^α are Laguerre polynomials. The frequency Ω now depends on the angle ϑ between the wiggler axis and the direction of the emitted photon according to

$$\Omega=\frac{\omega_0(\omega_0+2\omega)\rho}{\omega(1-\cos\vartheta)-\omega_0\cos\vartheta-p_v[\omega(1-\cos\vartheta)+\omega_0]/(h-m/4)} . \tag{A7}$$

For $\vartheta=0$, of course, this reduces to the on-axis result (23) with (24). For small angles $\vartheta \ll 1$ and $p_v \gg h$, Eqs. (A6) and (A7) reduce to

$$x=-\rho\frac{\sqrt{h}}{p_v}\frac{\omega_0-\frac{1}{2}\vartheta^2\omega}{\omega_0+\frac{1}{2}\vartheta^2\omega} , \tag{A8}$$

$$\Omega=-2\rho\frac{h}{p_v}\frac{\omega_0}{\omega_0+\frac{1}{2}\vartheta^2\omega}\omega . \tag{A9}$$

Although $x \ll 1$, it is not legitimate to let $x=0$ in Eqs. (A3) and (A4) since $m \gg 1$. Rather, the limit (see, e.g., Ref. 17)

$$\lim_{n\to\infty} L_n^{\alpha}\left[\frac{z}{n}\right]=n^{\alpha}x^{-\alpha/2}J_{\alpha}(2\sqrt{z}) \tag{A10}$$

has to be used. This leads to the following expression for the square of the matrix element M for fixed ρ and summed over the polarization of the emitted photon,

$$|M_{\rho}|^2=\frac{(2\pi)^5e^2L_vc^2\sin^2\vartheta}{\hbar L_T^2L_uV[\omega_0(\omega_0+2\omega)]^2\Omega}\frac{m!}{m'!}m^{m'-m}\delta(\mathbf{p}_T'-\mathbf{p}_T+\hbar\mathbf{K}_T)\delta\left[p_v'-p_v+\frac{\omega+\omega_0-\omega\cos\vartheta}{\omega_0(\omega_0+2\omega)}\Omega\right]$$
$$\times\delta\left[\tfrac{1}{2}(\nu-\nu')+\rho+\frac{(\omega+\omega_0)\cos\vartheta-\omega}{\omega_0(\omega_0+2\omega)}\Omega\right]\frac{1}{x^2}J_{m'-m}^2(2\sqrt{m}x)\left[\omega x-\frac{1}{2}\frac{\sqrt{h}}{p_v}(\omega+\omega_0)(m'-m)\right]^2 , \tag{A11}$$

where $m'-m=2\rho$. The last factor on the rhs of Eq. (A11) can be rewritten as ($\vartheta \ll 1$)

$$\omega x-\frac{1}{2}\frac{\sqrt{h}}{p_v}(\omega+\omega_0)(m'-m)=\frac{\Omega}{\sqrt{h}}\left[1+\frac{m}{4h-m}\frac{(\omega+\omega_0)(\omega_0+\frac{1}{2}\vartheta^2\omega)}{\omega_0(\omega_0+2\omega)}+\frac{h}{p_v}\frac{(\omega+\omega_0)(\omega_0+\frac{1}{2}\vartheta^2\omega)}{\omega_0(\omega_0+2\omega)}\right] , \tag{A12}$$

where the last two terms on the rhs are negligible.

---

*Permanent address: Facultad de Física, Pontifícia Universidad Católica de Chile, Casilla 6177, Santiago 22, Chile.

†Permanent address: Institut für Theoretische Physik, Universität Graz, A-8010 Graz, Austria.

[1]N. M. Kroll, P. L. Morton, and M. N. Rosenbluth, *Free-Electron Generators of Coherent Radiation,* Vol. 7 of *Physics of Quantum Electronics,* edited by S. F. Jacobs, H. S. Pilloff, M. Sargent III, M. O. Scully, and R. Spitzer (Addison-Wesley, Reading, MA, 1980), p. 147; N. M. Kroll, P. L. Morton, and M. N. Rosenbluth, IEEE J. Quantum Electron. **QE-17**, 1436 (1981).

[2]W. B. Colson, *Free-Electron Generators of Coherent Radiation,* Vol. 8 of *Physics of Quantum Electronics,* edited by S. F. Jacobs, G. T. Moore, H. S. Pilloff, M. Sargent III, M. O. Scully, and R. Spitzer (Addison-Wesley, Reading MA, 1982), p. 457.

[3]J. C. Goldstein, *Free-Electron Generators of Coherent Radiation,* edited by C. A. Brau, S. F. Jacobs, and M. O. Scully, Proc. Soc. Photo-Opt. Instrum. Eng. **453**, 2 (1984).

[4]W. B. Colson, Photo-Opt. Instrum. Eng. **453**, 290 (1984).

[5]C. M. Tang and P. Sprangle, Soc. Photo-Opt. Instrum. Eng. **453**, 11 (1984).

[6]W. B. Colson, Nucl. Instrum. Methods Phys. Res. A **250** 168 (1986).

[7]J. C. Goldstein, B. E. Newnam, R. W. Warren, and R. L. Sheffield, Nucl. Instrum. Methods Phys. Res. A **250**, 4 (1986); R. W. Warren, J. C. Goldstein, and B. E. Newnam, *ibid.* **250**, 19 (1986).

[8]J. Masud, T. C. Marshall, S. P. Schlesinger, and F. G. Yee, Phys. Rev. Lett. **56**, 1567 (1986).

[9]S. Riyopoulos and C. M. Tang, Nucl. Instrum. Methods A **259**, 226 (1987).

[10]J. M. J. Madey, J. Appl. Phys. **42**, 1906 (1971).

[11]W. Becker and J. K. McIver, J. Phys. (Paris), Colloq. **44**, C1-289 (1983).

[12]W. Becker and H. Mitter, Z. Phys. B **35**, 399 (1979).

[13]R. E. Langer, Am. Math. Soc. Trans. **36**, 637 (1934).

[14]W. Becker, Z. Phys. B **38**, 287 (1980).

[15]A. Bambini and A. Renieri, Lett. Nuovo Cimento **31**, 399 (1978); Opt. Commun. **29**, 24 (1978).

[16]J. Meixner and F. W. Schäfke, *Mathieu'sche Funktionen und Sphäroidfunktionen* (Springer, Berlin, 1954).

[17]*Handbook of Mathematical Functions,* edited by M. Abramowitz and I. A. Stegun (Dover, New York, 1965).

[18]C. Itzykson and J. B. Zuber, *Quantum Field Theory* (McGraw-Hill, New York, 1980).

[19]W. Becker and J. K. McIver, Z. Phys. D **7**, 353 (1988).

[20]W. E. Stein and R. L. Sheffield, Nucl. Instrum. Methods Phys. Res. A **250**, 12 (1986).

[21]J. K. McIver and M. V. Fedorov, Zh. Eksp. Teor. Fiz. **76**, 1996 (1979) [Sov. Phys.—JETP **49**, 1012 (1979)]; M. V. Fedorov and J. K. McIver, Phys. Lett. A **72**, 83 (1979).

[22]P. L. Kapitza and P. A. M. Dirac, Proc. Cambridge Philos. Soc. **29**, 297 (1933).

[23]M. V. Fedorov, Zh. Eksp. Teor. Fiz. **52**, 1434 (1967) [Sov. Phys.—JETP **25**, 952 (1967)]; W. Becker, R. Meckbach and H. Mitter, J. Phys. A **12**, 799 (1979); E. A. Coutsias and J. K. McIver, Phys. Rev. A **31**, 3155 (1985).

[24]W. Becker and J. K. McIver, Phys. Rep. **154**, 205 (1987).